

ULTRAVIOLET AND H α EMISSION IN ELLERMAN BOMBS

JIONG QIU, MING D. DING,¹ HAIMIN WANG, CARSTEN DENKER, AND PHILIP R. GOODE

Big Bear Solar Observatory, New Jersey Institute of Technology, 40386 North Shore Lane, Big Bear City, CA 92314-9672; qiu@bbso.njit.edu

Received 2000 July 6; accepted 2000 September 26; published 2000 November 9

ABSTRACT

We present the first high-cadence time profiles of Ellerman bombs (EBs) at two wavelengths, 1.3 Å in the blue wing of the H α line and the UV continuum at 1600 Å, and study their temporal correlation. Our results demonstrate that 46 out of 75 EBs exhibit a good correlation at the two wavelengths with a correlation coefficient greater than 50%, suggesting that a common energy release produces emission at the two wavelengths. We also find that the EBs with strong H α emission tend to show a good H α -UV correlation but that the weakly correlated or noncorrelated EBs are usually weak in H α emission. More than half of the H α -UV well-correlated EBs are located at the boundaries of unipolar magnetic areas; the others are located at, or close to, the magnetic inversion lines. However, the majority of the weakly or noncorrelated EBs are located at the magnetic inversion lines. Our results suggest that the physical mechanisms and the energy distributions are quite different in different types of EBs and that heating in the photosphere and temperature minimum region is very important for producing EBs. The high-cadence observations of EBs also confirm unambiguously that the light curves of EBs generally demonstrate a fast rise and a fast decay, with an average e -fold rising/decaying time of about 1 minute, which distinguishes EBs from the flare phenomenon.

Subject headings: Sun: activity — Sun: atmosphere — Sun: UV radiation

1. INTRODUCTION

For decades, Ellerman bombs (EBs; Ellerman 1917), or moustaches (Severny 1956, 1957, 1959), have been reported in observations of the chromosphere. They are fairly small, with a size of about 1", and tend to occur around sunspots or emerging flux regions. According to different observers, the mean lifetime of EBs is 11–14 minutes, and many of them recur (Engvold & Maltby 1968; Bruzek 1972; Roy & Leparskas 1973; Kurokawa et al. 1982; Zachariadis, Alissandrakis, & Banos 1987; Payne 1993; Denker et al. 1995; Dara et al. 1997; Nindos & Zirin 1998).

In the chromosphere, EBs are best observed in off-band H α filtergrams because they exhibit a much broadened line profile with significant emission up to a few angstroms off the line center, while the line center is a deep absorptive core (Kitai 1983). This indicates that EBs reside in the lower chromosphere. Observations also report a blue asymmetry in the H α and metallic line profiles (Severny 1959; Koval 1974), and this is interpreted as being due to either an upward motion of the emissive material from the deep chromosphere or a downward motion of the overlying absorptive material (Dara et al. 1997). Ding, Hénoux, & Fang (1998) suggested that the hydrogen line profiles of EBs can be produced by energetic electrons or protons preferentially originating in the lower atmosphere.

Studies also reveal the spatial coincidence of chromospheric EBs with photospheric facular points and granules (Bruzek 1972; Dunn & Zirker 1973; Wilson 1981; Kitai & Muller 1984; Zachariadis et al. 1987; Denker 1997). Kitai & Muller (1984) have shown that the contrast of EBs at H α – 0.75 Å is weakly correlated with enhanced facular features at a 4803 Å continuum. Vorpahl & Pope (1972) found that bright moustaches at 3840 Å reach the maximum about 3.5 minutes earlier than at H α – 0.9 Å. From these observations, it is suggested that upward-moving flux tubes from below may produce the gas heating that accounts for the EBs and correlated facular bright

points and that EBs may evolve with some phase difference in the photosphere and chromosphere. However, these conclusions are based on visual inspection, while a comparison of the time profiles at different wavelengths, to our knowledge, has never been presented. We also note that the above observations were made with a rather coarse temporal resolution. As we will show with our high-cadence observations, the time profiles of EBs generally demonstrate fast pulsations on time-scales of 1–5 minutes during their lifetimes of about 15 minutes, so it is important to compare the temporal behavior of EBs at different wavelengths with a time resolution that is much better than 1 minute.

In this Letter, we will present, for the first time, a comparative study of high-cadence time profiles of EBs observed at both the H α far wing and the UV 1600 Å continuum. The high-cadence observations at the Big Bear Solar Observatory (BBSO) are tuned at H α – 1.3 Å, and the observations at UV 1600 Å continuum are obtained from the *Transition Region and Coronal Explorer (TRACE)* (Handy et al. 1999). The two bands are formed at different heights in the atmosphere. The main contributor to the H α – 1.3 Å emission resides in the upper photosphere, while the narrowband UV 1600 Å continuum emission is mostly from the photoionization of Si I around the temperature minimum region (Vernazza, Avrett, & Loeser 1981). In a heated atmosphere, the minimum temperature can reach ~5000 K, in comparison with the quiet-Sun value of 4300 K. This requires an effective in situ heating mechanism in the lower atmosphere (Cook & Brueckner 1979). Study of the emission at these two wavelengths will help us understand the vertical structure of EBs and the heating of the lower atmosphere.

2. DATA REDUCTION

A high frame rate Silicon Mountain Design 1M-60 CCD camera is installed at BBSO for the purpose of high-cadence flare observations (Wang et al. 2000). On 2000 March 16, the active region NOAA 8906 (S16 W31) was observed continuously for a period of about 40 minutes, with a cadence of 0.1 s and a pixel size of 0".36. The image resolution was limited by seeing,

¹ Department of Astronomy, Nanjing University, 22 Hankou Lu, Nanjing, Jiangsu 210093, China.

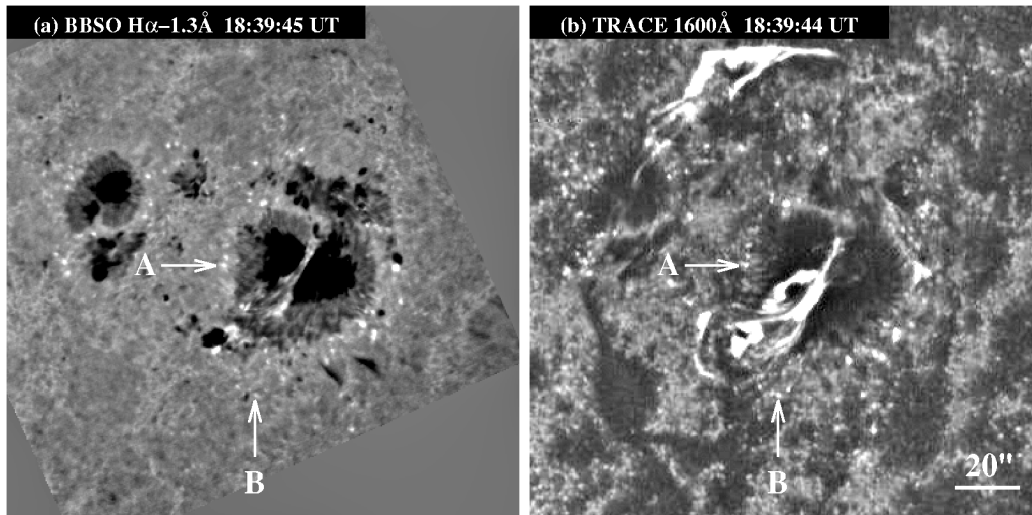


FIG. 1.—Filtergram of the active region NOAA 8906 at (a) 1.3 \AA in H α and at (b) 1600 \AA in the UV continuum

and the measurable size that was determined from the power spectrum of the quiet-Sun region was $0''.7\text{--}1''.1$ during the 40 minutes. The observations were made at 1.3 \AA in the blue wing of the H α line through a Lyot filter with a 0.25 \AA bandpass. Many EBs were observed around two sunspots (Fig. 1). To follow the temporal evolution of EBs, we examine the first frame of every 10 images, yielding about 2000 frames with a cadence of 1 s, and derive the light curves for the EBs. We first make dark-current and flat-field corrections for the images, and then we subtract the intensity of the quiet Sun from each image, normalize each frame to the quiet-Sun intensity, and co-align the images with a cross-correlation algorithm to subarcsecond accuracy. To identify EBs, we visually examine 200 of the 2000 images. In these 200 images, we interactively locate 75 bright points whose contrast is enhanced to be greater than 0.05. Then, in each of the 2000 frames, in a $3'' \times 3''$ box around each EB, the maximum intensity is found, and pixel values greater than 75% of the maximum are averaged. The mean position of these pixels is defined as the location of the EB. The light curves show the temporal evolution of the intensity contrast. We have tried various cutoff values to derive the intensity contrast. Since the maximum intensity of the EB may be sensitive to seeing variations, we also try to integrate the pixel values in a $3'' \times 3''$ box centered at the location of the EB in order to derive the H α flux light curve. These light curves with various cutoff values and different methods exhibit the same temporal trend, and the various cutoff values and methods do not alter the results of our subsequent analysis. In this Letter, we do not study the morphology; instead, we concentrate on the temporal behavior of EBs at different wavelengths. In the following sections, we use contrast light curves in both wavelengths with a 75% cutoff.

Targeting the same active region, *TRACE* observed the UV continuum at 1600 \AA with a varying cadence. From 18:20 to 18:50 UT, the cadence was 1–2 s, and afterward, the cadence changed to about 30 s. The pixel size of *TRACE* images is $0''.5$. The UV continuum and H α $- 1.3 \text{ \AA}$ images are co-aligned with subarcsecond accuracy (see Fig. 1), and the locations of the UV counterparts of the EBs are determined. The data are calibrated (R. N. Nightingale 2000, private communication) and normalized. An accurate flat-field pattern for our *TRACE* observations is not available (R. N. Nightingale 2000, private communication), so we do not apply a flat-field correction to

the UV images. However, since the pixel-to-pixel variation of the CCD response is small, this does not affect the time profiles of EBs that are fairly small. Furthermore, the image shift relative to the CCD image plane, due to solar rotation during 40 minutes, can only produce a $\leq 1\%$ variation in the light curve of an individual EB. By comparing the intensities of many quiet regions distributed across the field of view (FOV), we estimate a less than 10% variation in the flat-field pattern. The UV time profiles of the EBs are computed using the same method that we use to compute the H α light curves.

3. RESULTS

Figure 2 illustrates the light curves of two characteristic EBs at both H α $- 1.3 \text{ \AA}$ and UV 1600 \AA continuum. The majority of the 75 examined EBs have a lifetime between 10 and 20 minutes, in agreement with previous observations (Kurokawa et al. 1982). Many of them recur even during the 40 minutes of observations, but the recurring EBs usually do not have the same lifetimes. From our high-cadence observations, we also find that the light curves of almost all observed EBs show fine structures at various timescales ranging from 1 to 5 minutes, as shown in Figure 2. These temporal structures are not due to seeing variations, because they can be seen in both H α off-band and UV continuum emission. We also examine the rising/decaying time of individual EBs. For this purpose, we select EBs with well-observed rising and decaying phases and compute the e -fold rising and decaying times. Because EB emission shows multiple spikes, we consider only the first spike to compute the rising time and the last spike to compute the decaying time. The e -fold rising/decaying time is defined as the time between the maximum of the spike and the time when the emission increases/decreases to $1/e$ of the maximum. To eliminate seeing effects, we use a Fourier filter to remove variations faster than 1 minute. For 81 such light curves, including all recurring components, the mean rising time is $64 \pm 34 \text{ s}$, and the mean decaying time is $73 \pm 35 \text{ s}$. Because of the existence of successive fine structures in the EB light curves, the real rising and decaying times may actually be shorter. However, it is still safe to say that typical EBs demonstrate an impulsive rise and a comparably fast decay and that the decaying time is not significantly longer than the rising time. In

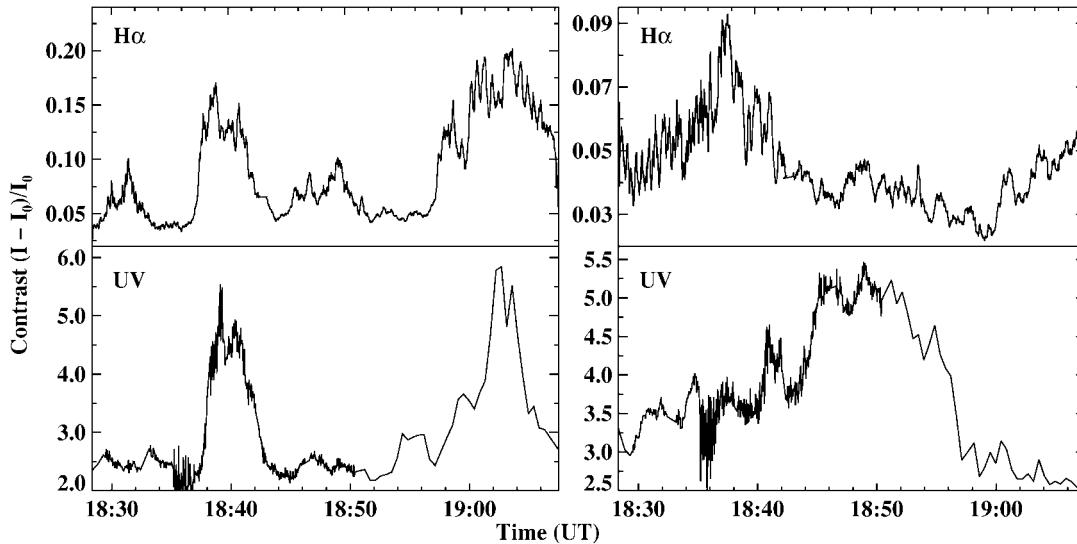


FIG. 2.—Time profiles of two characteristic EBs at 1.3 \AA in $H\alpha$ and at 1600 \AA in the UV continuum demonstrating a correlated case (*left*), $r_t = 0.81$, denoted A in Fig. 1, and a noncorrelated case (*right*), $r_t = -0.06$, denoted B in Fig. 1.

fact, the time profiles of more than 60% of the EB components look fairly symmetric about the maxima.

Many EBs exhibit a temporal correlation between the $H\alpha$ and UV light curves. In Figure 2, we demonstrate one case of good correlation and one case of noncorrelation. To study the temporal correlation between $H\alpha$ and UV emission, we interpolate the time profiles in both wavelengths into an evenly spaced time grid and compute their linear cross-correlation. To reduce seeing effects, the $H\alpha$ time profiles used for interpolation are ten-point-smoothed. The histogram in Figure 3 shows the distribution of the $H\alpha$ -UV correlation. The correlation between $H\alpha$ and UV emission is generally good. During 40 minutes of observations, among 75 EBs, 67 EBs have a positive correlation coefficient, and 46 EBs demonstrate a correlation coefficient greater than 50%. Only eight EBs do not show a correlation at all (i.e., a negative coefficient). This suggests that a common energy release process produces the emission in the two spectral ranges. We also apply a sequence of time delays, ranging from 1 to 200 s, to the computation of the cross-correlation coefficient. We cannot find any characteristic time delay that improves the correlation. Therefore, there is virtually no time delay between the light curves in the

two wavelengths. This result is in disagreement with Vorpahl & Pope (1972), who claimed that the bright points at 3840 \AA reach the emission maximum ahead of chromospheric $H\alpha$ moustaches by 3.5 minutes. In our observations, we do not find any phase difference in the evolution of EBs in the $H\alpha$ far wing and UV continuum. This does not support the scenario, as suggested by Kitai & Muller (1984), that there is a phase difference in the evolution of EBs in different atmospheric levels.

According to the $H\alpha$ -UV temporal correlation coefficient r_t , we classify the EBs into three groups: (1) 46 EBs with $r_t > 50\%$ are regarded as well-correlated cases, (2) 21 EBs with a positive $r_t < 50\%$ are regarded as weakly correlated cases, and (3) eight EBs with a negative r_t are regarded as uncorrelated cases. We examine the $H\alpha$ and UV contrast distribution. For each EB, in both $H\alpha$ and UV, out of 2390 time frames, we take the mean of the 239 brightest frames as the time-averaged contrast (TAC) during the 40 minutes. Figure 4 gives the scatter plot of the UV TAC against the $H\alpha$ TAC for the EBs in the first group. There is a linear trend in the scatter plot, but the contrast correlation r_c is not very strong, $r_c = 43\%$. In the other

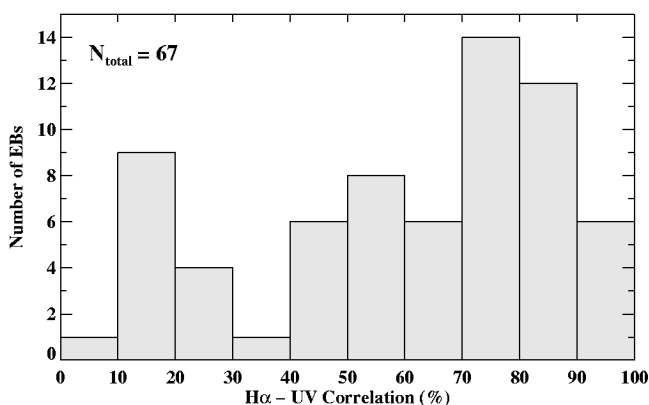


FIG. 3.—Correlation distribution. In the histogram, eight EBs with a negative correlation coefficient are not counted.

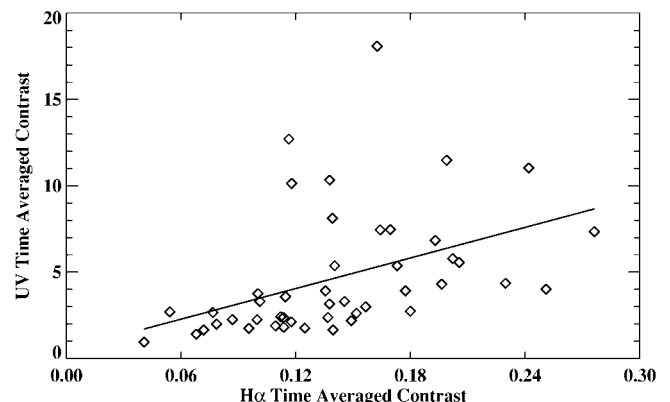


FIG. 4.—Scatter plot of the UV TAC vs. the $H\alpha$ TAC in group 1. Each point (*diamond*) denotes one EB. The straight line gives the least-squares linear fit to the data.

two groups, r_c is even smaller, $r_c = 26\%$ and -31% for the second and third group, respectively. But considering that the nonuniformity of the UV CCD response across the FOV is at the level of 6%–7%, the scatter plot may not be very accurate. We also find that the mean H α TAC, denoted as C_H , of the well-correlated EBs is generally higher than the other two groups. For the three groups, C_H is 0.14 ± 0.05 , 0.09 ± 0.05 , and 0.08 ± 0.01 , respectively. This indicates that when the H α emission is not strong, the H α -UV correlation is weak.

In Figure 5, we show the locations of EBs on the longitudinal magnetogram. During the observations, we do not detect changes in the magnetic field. In Figure 5, we integrate 10 frames of magnetograms taken in good seeing condition from 18:28 to 18:55 UT. We find that 38 out of 75 EBs are located at the boundaries of single magnetic polarities and that the other 37 are located at or close to the magnetic inversion lines dividing two opposite magnetic polarities. When we relate the locations of EBs to their temporal properties in H α and UV, the result is very interesting. In the first group, out of 46 EBs, 28 are at the boundaries of unipolar areas, and 18 are at the inversion lines, while in the other 29 EBs, 10 are at the boundaries of unipolar areas, and 19 are at the inversion lines. Therefore, the majority of H α -UV well-correlated EBs are related to unipolar magnetic configurations, while the majority of weakly or noncorrelated EBs are associated with the magnetic inversion line configurations. This suggests that the mechanisms for the two types of EBs may be quite different.

4. DISCUSSION AND CONCLUSION

We find that the light curves of EBs usually show a fast rise and a fast decay, with a comparable rising time and decaying time of about 1 minute. Many EB light curves are almost symmetric about the flat maximum plateau consisting of many spikes. This is quite different from flare light curves, which typically exhibit a fast rise and a gradual decay. The same conclusion was reached by previous studies (Zachariadis et al. 1987; Payne 1993; Nindos & Zirin 1998), but our observations strongly confirm this point with the least ambiguity owing to the high cadence in our observations.

From our observations, we also establish a clear temporal correlation in the emission in the H α far wing and UV continuum for the majority of bright EBs. This is a strong indication that the EB radiation in these two bands shares a common energy source. From limb observations, Harvey (1963) found that the height of an EB observed at H $\alpha - 1 \text{ \AA}$ is 400 km above the photosphere. The formation height of the H $\alpha - 1.3 \text{ \AA}$ emission used in the present observations is slightly lower. Enhanced emission in both the H α far wing and the UV 1600 \AA continuum indicates an efficient heating process in the lower atmosphere. Theoretically, there is still an ambiguity concerning the mechanism for the greatly enhanced H α far wing emission, but our results provide evidence that the heating source must be located close to the temperature minimum region and that these bright EBs have a vertical span of a few hundred kilometers.

We also find that EBs that are brighter in the H α emission tend to exhibit a good H α -UV correlation. These bright H α EBs must be produced by a heating source sitting in or penetrating into the very deep atmosphere. On the other hand, the H α emission of the weakly or noncorrelated EBs is weak, so in these EBs, the heating of the lower atmosphere is not strong compared with EBs with good H α -UV correlations. For these weakly or noncorrelated EBs, we also need to investigate the

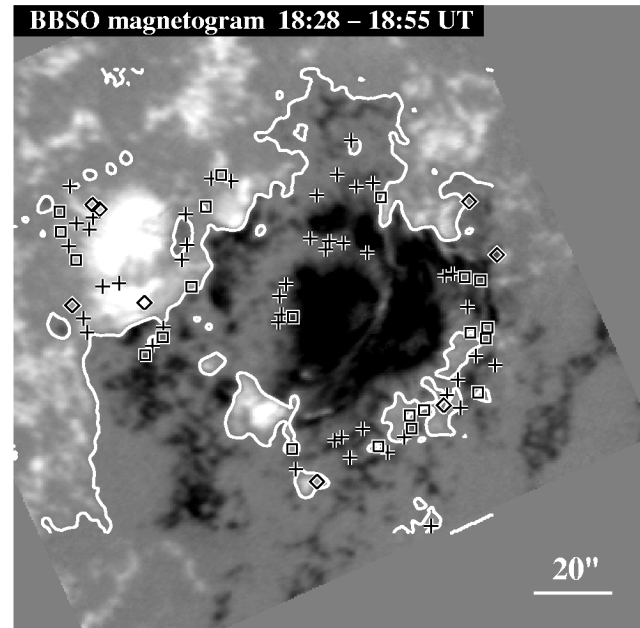


FIG. 5.—Locations of EBs on the longitudinal magnetogram. The plus signs, squares, and diamonds indicate EBs from groups 1, 2, and 3, respectively. The thick solid lines indicate the inversion lines of the longitudinal magnetic field.

following questions: Are the H α and UV enhancements produced by the same or different heating sources? If they are produced by different energy release processes, are these processes possibly triggered by one another?

To some observers, the spatial coincidence of chromospheric EBs and photospheric facular bright points helped reinforce the idea that an EB is a small magnetic flux tube moving upward to compress the dense atmosphere (Vorpahl & Pope 1972; Kitai & Muller 1984). This is challenged by observations demonstrating that EBs are not located at the center of small magnetic elements. For EBs at the magnetic inversion lines and for those associated with emerging bipoles, the magnetic reconnection in the lower chromosphere may be an agent of gas heating. However, more than half of the H α -UV well-correlated EBs in our observations are located at the boundaries of single magnetic polarities. Nindos & Zirin (1998), in a separate study, also suggest that EBs are not related to approaching opposite polarities. We note that in other studies, some UV microflares are also located in unipolar areas (Wang et al. 1999). Our results also show that EBs located at the magnetic inversion lines seem to exhibit different H α -UV temporal properties from those in the unipolar areas. These findings suggest that there are different mechanisms for different types of EBs, and for many EBs and other small-scale brightenings, the photospheric process must play an important role.

The authors are grateful to Richard N. Nightingale for help with the *TRACE* calibration and Eugene H. Avrett for helpful discussions. We thank the BBSO observing staff and the *TRACE* team for data support. We also thank the referee for very helpful comments and suggestions. The work is supported by the NSF under grants ATM-9714796 and ATM-0076602, by NASA under grants NAG5-9682, NAG5-7837, and NAG5-9501, and by the ONR under grant N00014-97-1-1037.

REFERENCES

- Bruzek, A. 1972, *Sol. Phys.*, 26, 94
Cook, J. W., & Brueckner, G. E. 1979, *ApJ*, 227, 645
Dara, H. C., Alissandrakis, C. E., Zachariadis, Th. G., & Georgakilas, A. A. 1997, *A&A*, 322, 653
Denker, C. 1997, *A&A*, 323, 599
Denker, C., de Boer, C. R., Volkmer, R., & Kneer, F. 1995, *A&A*, 296, 567
Ding, M. D., Hénoux, J.-C., & Fang, C. 1998, *A&A*, 332, 761
Dunn, R. B., & Zirker, J. B. 1973, *Sol. Phys.*, 33, 281
Ellerman, F. 1917, *ApJ*, 46, 298
Engvold, O., & Maltby, P. 1968, in *Nobel Symp. 9, Mass Motion in Solar Flares and Related Phenomena*, ed. Y. Ohman (New York: Wiley), 109
Handy, B. N., et al. 1999, *Sol. Phys.*, 187, 229
Harvey, J. W. 1963, *Observatory*, 83, 37
Kitai, R. 1983, *Sol. Phys.*, 87, 135
Kitai, R., & Muller, R. 1984, *Sol. Phys.*, 90, 303
Koval, A. N. 1974, *Izv. Krymskoi Astrofiz. Obs.*, 52, 100
Kurokawa, H., Kawaguchi, I., Funakoshi, Y., & Nakai, Y. 1982, *Sol. Phys.*, 79, 77
Nindos, A., & Zirin, H. 1998, *Sol. Phys.*, 182, 381
Payne, T. 1993, Ph.D. thesis, New Mexico State Univ.
Roy, J.-R., & Leparskas, H. 1973, *Sol. Phys.*, 30, 449
Severny, A. B. 1956, *Izv. Krymskoi Astrofiz. Obs.*, 16, 194
———. 1957, *Izv. Krymskoi Astrofiz. Obs.*, 17, 129
———. 1959, *Izv. Krymskoi Astrofiz. Obs.*, 21, 131
Vernazza, J. E., Avrett, E. H., & Loeser, R. 1981, *ApJS*, 45, 635
Vorpahl, J., & Pope, T. 1972, *Sol. Phys.*, 25, 347
Wang, H., Chae, J., Qiu, J., Lee, C.-Y., & Goode, P. R. 1999, *Sol. Phys.*, 188, 367
Wang, H., Qiu, J., Denker, C., Spirock, T., Chen, H., & Goode, P. R. 2000, *ApJ*, 542, 1080
Wilson, P. R. 1981, *Sol. Phys.*, 69, 9
Zachariadis, Th. G., Alissandrakis, C. E., & Banos, G. 1987, *Sol. Phys.*, 108, 227